Investigation of a SP/S Resonant Compensation Network Based IPT System with Optimized Circular Pads for Electric Vehicles

Chenglian Ma[†], Shukun Ge[*], Ying Guo[**], Li Sun[*], and Chuang Liu[*]

[†,*]School of Electrical Engineering, Northeast Dianli University, Jilin, China
[**]State Grid Zibo Power Supply Company, Zibo, China

Abstract

Inductive power transfer (IPT) systems have become increasingly popular in recharging electric vehicle (EV) batteries. This paper presents an investigation of a series parallel/series (SP/S) resonant compensation network based IPT system for EVs with further optimized circular pads (CPs). After the further optimization, the magnetic coupling coefficient and power transfer capacity of the CPs are significantly improved. In this system, based on a series compensation network on the secondary side, the constant output voltage, utilizing a simple yet effective control method (fixed-frequency control), is realized for the receiving terminal at a settled relative position under different load conditions. In addition, with a SP compensation network on the primary side, zero voltage switching (ZVS) of the inverter is universally achieved. Simulations and experiments have been implemented to validate the favorable applicability of the modified optimization of CPs and the proposed SP/S IPT system.

I. INTRODUCTION

The trend towards the development of plug-in hybrid electric vehicles (PHEVs) and pure EVs for transportation will continue to grow due to its advantages in terms of energy saving, low pollution and low-carbon emissions [1], [4]. Wireless Power Transfer (WPT) systems recharge EVs wirelessly by means of high frequency magnetic field coupling [1], [2], [4]-[6]. WPT systems are more convenient and safer than plug-in charging systems since they are free from the plug wire arc phenomenon and electrical shocks. Moreover, WPT systems can operate in a variety of bad types of weather and environment such as rain and snow [2], [7].

Lately, IPT has become the most prevailing technique in WPT systems, and this is also adopted in this paper. In an IPT system the power transfers from the transmitting terminal to the receiving terminal through a large air gap (1-20 cm) with a loose electromagnetic coupling between separate primary (transmitting) and secondary (receiving) coils. The two coils are usually installed underground and in the EV's chassis, respectively [7]-[17]. The predominant limiting factor that affects the transfer capacity of the effective power is the magnetic coupling coefficient of the magnetic structure [4]-[5], [11], [12]. In an IPT system, the magnetic structure is usually designed as two pads. The very early designs of pads usually used U-shape cores [18], ferrite plates [19], [20], pot cores [21], or E-cores [22]. These designs need large-sized ferrite cores to form a magnetic flux path, and they could only transfer power through a very small gap. The designs using pot cores, U-shape cores or E-cores are necessarily thick, which is a problem when it comes to chasis requirements [5], [17], [18], [21], [22]. In order to solve this problem, some new magnetic structures have been presented in [1], [2], [9]-[12], [23], [24]. Two classical pad designs are commonly used in IPT systems. One is the Double-D pad (DDP) [12], [23]-[24]. The other one is the CPs [2], [11]. Both of them were proposed by the University of Auckland. The CPs is chosen in this paper and further optimization of the CPs has been done. After this optimization, the magnetic coupling coefficient and power transfer capacity are
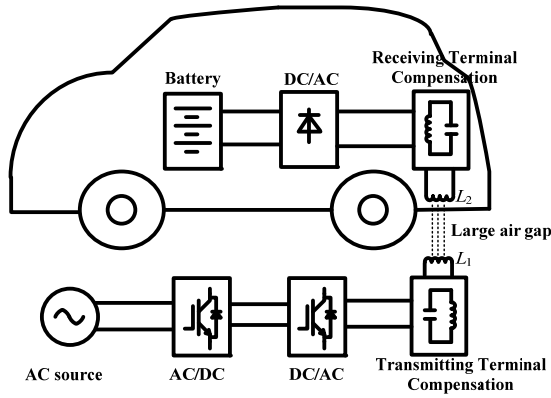
Fig. 1. Typical inductive wireless charging system for EVs.

dramaticly improved as shown in section II.

A typical IPT system for EV charging is shown in Fig. 1. First, AC voltage is converted to DC voltage by an AC-DC rectifier. Then, the DC voltage is transformed into a high frequency square wave voltage by a DC-AC inverter to drive the transmitting coil through a compensation network. The high frequency alternating current in the transmitting coil generates an alternating magnetic field, which induces an AC voltage on the receiving coil. Finally, AC power is rectified to charge the batteries in EVs [1], [2], [9], [10].

The output power (P_{out}) of an IPT system is determined by the open circuit voltage (V_{oc}), the short circuit current (I_{sc}) of the receiver pad and the quality factor of the receiver circuit (Q_2), as shown in Eq. (1) [13].

$$P_{out} = P_{su}Q_2 = V_{oc}I_{sc}Q_2$$
$$= \omega M I_1 \frac{M I_1}{L_2} Q_2 = \omega I_1^2 \frac{M^2}{L_2} Q_2 . \qquad (1)$$

Where P_{su} represents the power transferred to the receiver pad and is defined as:

$$P_{su} = V_{oc}I_{sc} . \qquad (2)$$

$V_{oc}=j\omega M I_1$ (ω is the angular frequency of the transmitting coil current I_1, and M is the mutual inductance between the two coils), and L_2 represents the self-inductance of the receiver coil [11], [12]. In practical applications, the quality factor Q_2 is constrained below 6 [9], [10], [12], and if ω and I_1 are constant [9], [13], [16] it can be derived from Eq. (1) that P_{out} will only be dependent on M^2/L_2. The magnetic coupling coefficient k can be determined by Eq. (3), where L_1 represents the self-inductance of the transmitting coil.

$$k = \frac{M}{L_1 L_2} . \qquad (3)$$

In an IPT system, the two pads are loosely coupled. It is required to use a resonant compensation network before the transmitting pad to reduce the VA rating [1], [3], [4], [9]. Four basic resonant topologies: series-series (SS), series-parallel (SP), parallel-series (PS), and parallel-parallel (PP) are widely known [1], [7], [9], [23], [24]. For the transmitting side, S and P resonant compensation networks

are in common use. S resonant compensation networks make it easier to control the parameters and bring a lower THD. P resonant compensation networks can act as a current source. Previous researchers chose S or P resonant compensation networks for special issues such as control, harmonic or efficiency [1], [23]. Recently, SP resonant compensation networks for the transmitting terminal have been widely proposed because they can behave as a constant current source and have the performance of unity-power-factor [14], [25]-[27]. For the rece, ving terminal, P resonant compensation networks are often used due to their output characteristic of constant current source [1], [2], [28], [29]. On the other hand, with a S resonant compensation network an IPT system can achieve a constant voltage output without constant-voltage control, which is ideal for EV battery charging. On this occasion, the regulation of the output voltage can be realized by adding a DC/DC circuit.

Output power is usually controlled with variable frequency operation. However, this has several disadvantages including the noise spectrum, more complex filtering, poor magnetic structure utilization and loss of ZVS operation which is normally preferred [1], [7], [8]. These shortcomings can be resolved with a fixed-frequency control (the switch frequency is constant) which is simple but effective [1], [13]. With fixed-frequency control, the system has more advantages such as no bifurcation phenomenon, simple control structure, ZVS operation of the inverter switches and so on [1], [13]. Therefore, fixed-frequency control is chosen in this paper.

This paper is organized as follows. Section II presents the further modified optimization process of CPs based on a previous study [11]. Section III analyzes the proposed SP/S resonant compensation network for IPT systems. In section IV, a 6.6 kW prototype with the optimized CPs is mounted to validate the correctness and effectiveness of the optimization results and the proposed SP/S resonant compensation network. Finally, some conclusions are drawn in section V.

II. MODIFIED OPTIMIZATION PROCESS OF CPS

A. Optimization of the Mean Coil Radius

CPs has been optimized by the University of Auckland as shown in Ref. [11], and they are generally used as the IPT systems' magnetic structures. Here a further optimization of CPs is based on the former research. A 600-mm-diameter CPs imitating the previous conclusions is designed as shown in Fig. 2(a). The 26 turns' coil (bifilar 13 turns) is composed of AWG38 Litz wire (1050 strands). Each ferrite bar consists of nine TDG I79/24/4 mm cores, so that the dimensions of every bar are 237/24/12 mm. However, simulation results obtained with Finite Element Analysis (FEA) software from Ansoft indicate that the conclusions in Ref. [11] are optimal except for the mean coil radius. Thus, further optimization of the mean coil radius is what needs to be done next. Here, the
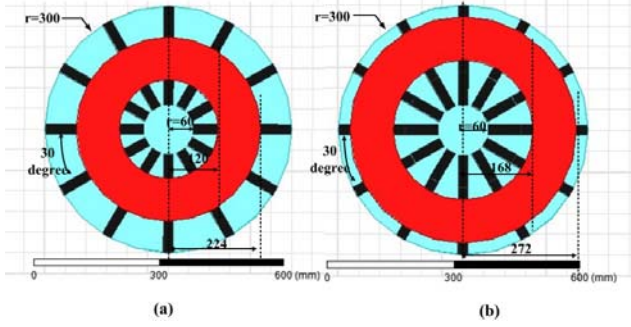
Fig. 2. Pad dimensions in mm (a) Following Ref. [11], (b) After further optimization.
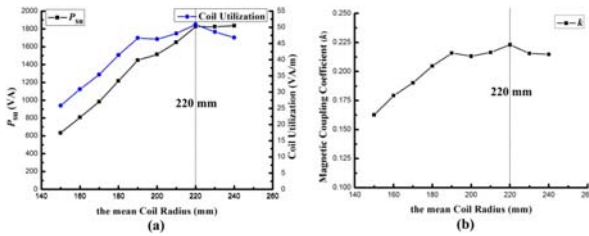

Fig. 3. Parameters against mean coil radius under the transmitting coil excitation of 40A at 20 kHz (200 mm gap and no horizontal misalignment) (a) P_{su} and coil utilization, (b) Magnetic coupling coefficient k.

uncompensated power P_{su} and magnetic coupling coefficient $k=M/L_1L_2$ are used to make comparisons among the different designs of CPs. In addition, for the first time, coil utilization (CU) is defined in this paper as another comparison reference among different CPs. CU is equal to the quotient of P_{su} and the coil's blank length (L), as is expressed in equation (4).

$$CU = \frac{P_{su}}{L} . \tag{4}$$

Fig. 3 shows the variations of the uncompensated power P_{su}, coil utilization CU, and magnetic coupling coefficient k against the mean coil radius with a 200 mm gap and no horizontal misalignment, given that the transmitting coil excitation is a 20 kHz current source of 40 RMS (the same excitation as below). When mean coil radius ranges between 140 and 220 mm, all of them (P_{su}, k and CU) increase rapidly with the growth of the mean coil radius. However, when it is above 220 mm, the rising rate of P_{su} becomes slow while k and CU are inversely proportional to the mean coil radius. Thus, taking these various factors into consideration, the optimal mean coil radius is 220 mm which accounts for 73% of the CPs radius not the 53% in Ref. [11]. The further optimized CPs' dimensions are shown in Fig. 2 (b).

B. Comparisons of Previous and the Optimized CPs

In order to validate the effectiveness and correctness of the optimization, k and P_{su} are assessed between the imitating CPs (represented by 1) and the optimized ones (represented by 2) with different horizontal and vertical misalignments. Fig. 4(a) shows the line trend of k and P_{su} against horizontal
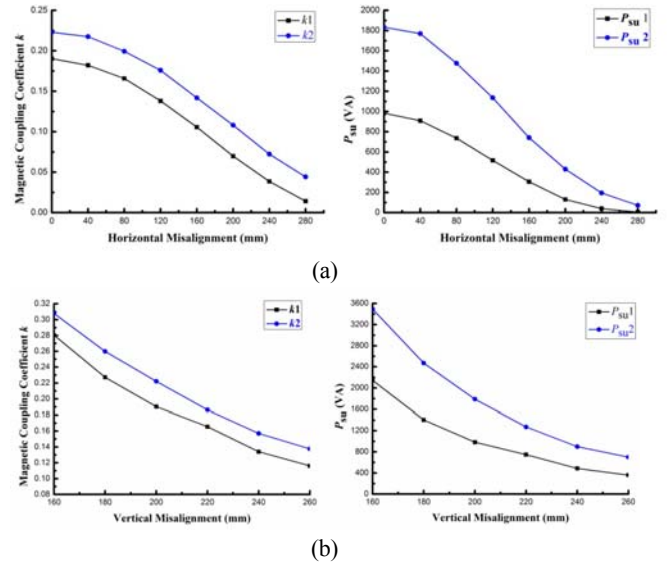

(a)

(b)

Fig. 4. k and P_{su} against horizontal and vertical misalignment under the excitation of 40 A at 20 kHz. (a) Against horizontal misalignment (200mm gap), (b) Against vertical misalignment (no horizontal misalignment).

misalignment (200 mm gap). Compared with previous CPs, both k and P_{su} are improved significantly. With no horizontal misalignment, k and P_{su} get a growth of 0.03 and 850 VA, respectively. Fig. 4(b) shows the same two variables against vertical misalignment (no horizontal misalignment). Similarly, both k and P_{su} are enhanced tremendously.

C. Meeting Regulations of the Leakage Magnetic Field

In order to meet the application requirements for EVs recharging, CPs should ideally comply with the International Commission on Non-Ionizing Radiation Protection guidelines (ICNIRP). ICNIRP stipulates that the average RMS flux density of the body exposure should be below 6.25 μT for the general public in the frequency range from 0.8 to 65 kHz [30]. When it comes to measurement techniques, the standard also includes a body average, spot limits and a temporal average. Spot limits can be $\sqrt{20}$ times the exposure level. As a result, the maximum exposure level is 27.9 μT for the general public in the frequency range from 0.8 to 65 kHz [31]. Above all, the spot limits for the general public must be held under 27.9 μT in this paper. As is shown in Fig. 5, Ansoft Simulation results are used to estimate the leakage magnetic field around the CPs under a transmitting coil excitation of 40 A at 20 kHz with a 200 mm gap and no horizontal misalignment. It is well known that an EV's width is generally around 2000 mm. A leakage field of 800 mm (less than half of the average EV's width) away from the axis of the CPs is presented. The maximum spot flux density is 25.7 μT at a distance of 800 mm from the center of the CPs. One illustrated 1.8 m tall person is standing 800 mm away from the CPs' axis, and the simulated results of the body exposed flux density are shown in Fig. 5. It can be easily seen that the IPT system in this
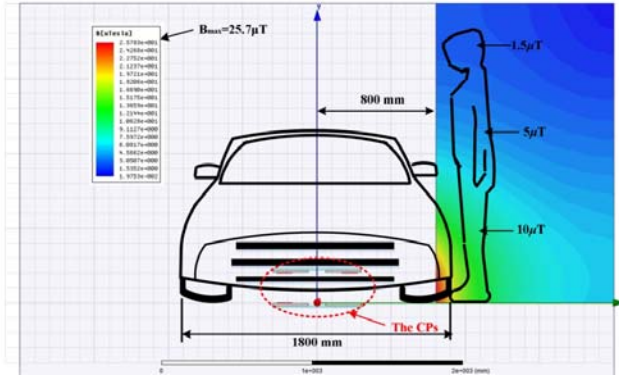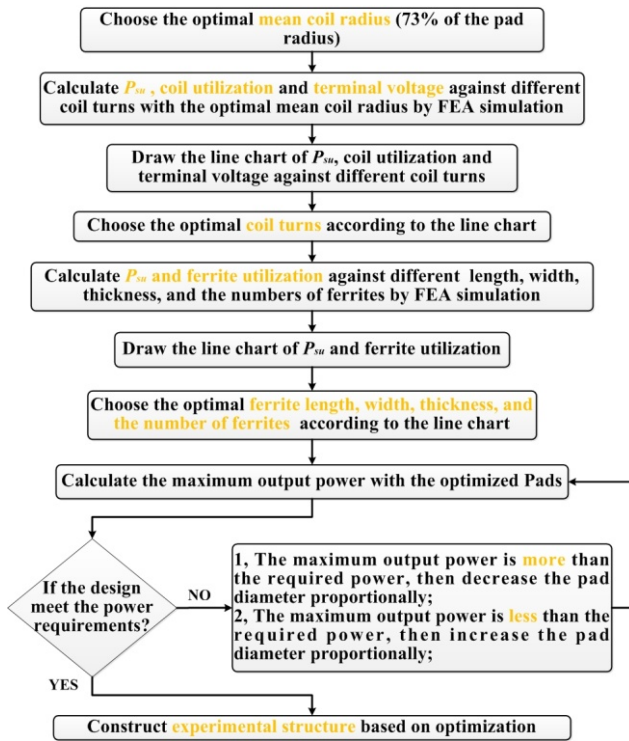
Fig. 5. Simulation results of the leakage field.

ig. 6. Flow diagram of the design and optimization process.

paper can commendably meet the ICNIRP stipulations.

D. Design and Optimization Approach of the CPs

According to the analysis above and previous research in Ref. [11], the design and optimization approach is shown in Fig. 6. Based on the EVs charging demands, an initial assumed model is investigated to determine key factors such as the coil turns, mean coil radius, and ferrites' length, width, thickness, and numbers through the FEA simulation. Finally, the favorable experimental CPs with optimal parameters can be received.

III. THE SP/S RESONANT COMPENSATION NETWORK

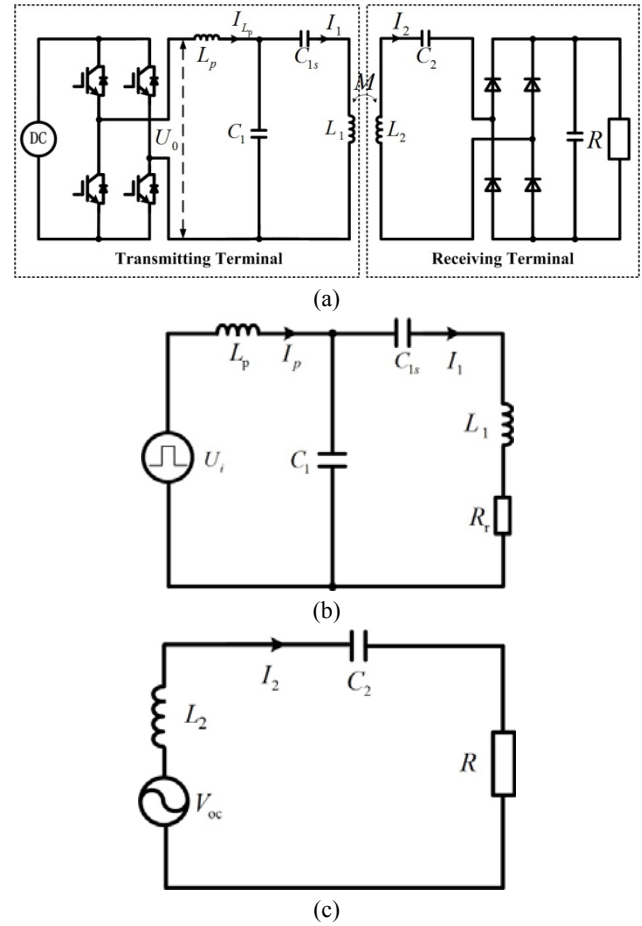The SP/S equivalent resonant compensation network

(a)

(b)

(c)

Fig. 7. The IPT system equivalent network (a) SP/S resonant compensation network, (b) Equivalent circuit of transmitting terminal, and (c) Equivalent circuit of receiving terminal.

shown in Fig. 7(a) is proposed for IPT systems with optimized CPs based on the analysis in section II.

A. SP Resonant Compensation Network for the Transmitting Terminal

The equivalent circuit of a SP resonant compensation network for the transmitting terminal is shown in Fig. 7(b), where R_r represents the reflected impedance from the secondary to the primary. The receiving terminal can be purely resistive as discussed in part B. Thus, the reflected impedance can be represented by R_r. An additional capacitor C_{1s} is added in series with the transmitting coil self-inductance L_1, which allows for a greater constant current in the transmitting coil and improves the excitation intensity.

The resonant frequency ω_0 and the normalized switching frequency ω_n are defined as:

$$\omega_0 = \frac{1}{\sqrt{L_p C_1}} \ , \ \omega_n = \frac{\omega}{\omega_0} \ . \tag{5}$$

The quality factor Q_1 of the transmitting network is:

$$Q_1 = \frac{\omega_0 L_p}{R_r} \ . \tag{6}$$

The ratio of L_p to L_1 is given by:

$$\lambda = \frac{L}{L_p}. \tag{7}$$

Here L is the equivalent inductance determined by:

$$L = L_1 - \frac{1}{\omega^2 C_{1s}}. \tag{8}$$

Then the current flowing through the transmitting coil can be derived as:

$$
\begin{aligned}
I_1 &= \frac{U_i}{j\omega L_p + (1/j\omega C_1)//(j\omega L + R_r)} \cdot \\
&\quad \frac{1/j\omega C_1}{1/j\omega C_1 + (j\omega L + R_r)} \\
&= \frac{U_i}{j\omega\left[L_p + (L + R_r/j\omega)(1-\omega_n^2)\right]}
\end{aligned} \tag{9}
$$

When the switching frequency is equal to the resonant frequency $1-\omega_n^2=0$, the transmitting coil current can be expressed as Eq. (10), which is independent of Q_1.

$$I_1 = \frac{U_i}{j\omega L_p} \tag{10}$$

The input impedance for the transmitting terminal can be derived as:

$$
\begin{aligned}
Z_1 &= j\omega L_p + (1/j\omega C_1)//(jwL + R_r) \\
&= \frac{\omega_0 L_p\left\{(1-\omega_n^2) + jQ_1\omega_n\left[1+\lambda(1-\omega_n^2)\right]\right\}}{Q_1(1-\lambda\omega_n^2) + j\omega_n}.
\end{aligned} \tag{11}
$$

Set the inverter output voltage's initial phase angle at 0 degrees, and the inverter output current can be derived as:

$$
\begin{aligned}
I_p &= \frac{U_i}{Z_1} \\
&= U_i \cdot \frac{Q_1(1-\lambda\omega_n^2) + j\omega_n}{\omega_0 L_p\left\{(1-\omega_n^2) + jQ_1\omega_n\left[1+\lambda(1-\omega_n^2)\right]\right\}}.
\end{aligned} \tag{12}
$$

When switching frequency is equal to the resonant frequency $1-\omega_n^2=0$, Eq. (12) can be simplified as:

$$I_p = \frac{U_i}{Z_1} = \frac{U_i}{\omega_0 L_p}\cdot\left[\frac{1}{Q_1} + j(\lambda-1)\right]. \tag{13}$$

Therefore, the phase angle between the inverter output voltage and current can be derived as:

$$
\begin{aligned}
\varphi|_{\omega_n=1} &= \arctan\left[Q_1(\lambda-1)\right] \\
\varphi|_{\omega_n=1} &= 0, \lambda=1 \\
\varphi|_{\omega_n=1} &< 0, \lambda<1 \\
\varphi|_{\omega_n=1} &> 0, \lambda>1
\end{aligned} \tag{14}
$$

In the end, the inverter can operate in the lagging power-factor mode if $\lambda<1$. Then the antiparallel diodes conduct prior to the switch so that the ZVS operation is realized [14], [25]-[27].
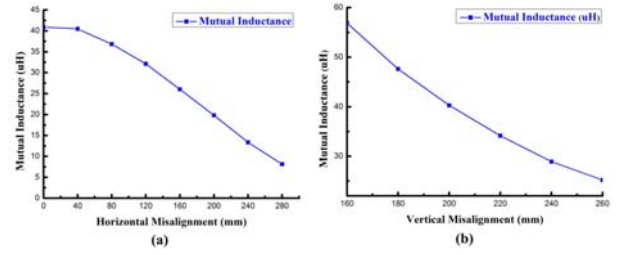

Fig. 8. Measured mutual inductance of optimized CPs (a) Against horizontal misalignment, (b) Against vertical misalignment.

B. S Resonant Compensation Network of the Receiving Terminal

The equivalent circuit of the S resonant compensation network for receiving terminal is shown in Fig. 7(c). The receiving coil self-inductance L_2 is in series resonant with C_2 at the resonant frequency ω_0. $V_{oc}=j\omega MI_1$ is the effective voltage induced in the receiving coil by I_1 through mutual coupling. It can be seen from Eq. (10) that I_1 is independent of the load. Naturally V_{oc} can also be regarded as a constant.

The input impedance Z_2 for the receiving terminal can be derived as Eq. (15) when $1-\omega_n^2=0$. In this case, Z_2 is pure resistance.

$$Z_2 = j\omega L_2 + 1/j\omega C_2 + R = \frac{\left(1-\omega_n^2\right)L_2 C_2}{j\omega C_2} + R = R. \tag{15}$$

The voltage across the load can be expressed as:

$$U_R = \frac{R}{j\omega L_2 + 1/j\omega C_2 + R}\cdot V_{oc} = V_{oc} = j\omega MI_1. \tag{16}$$

Then the voltage gain Gv can be given by:

$$G_v = \frac{U_R}{U_0} = \frac{j\omega MI_1}{U_0} \tag{17}$$

The voltage gain G_v is independent of R and increases in proportion to the mutual inductance M. When the relative position of two pads is confirmed, the mutual inductance can be determined as shown in Fig. 8, and the voltage gain G_v becomes constant.

IV. EXPERIMENTAL RESULTS

A. The Experimental Parameters

In order to demonstrate the effectiveness and correctness of the optimized CPs and the analysis of the proposed SP/S resonant compensation network, a complete experimental prototype has been built. The CPs follow the optimization results from Section II, as shown in Fig. 9(a), and the experimental prototype is displayed in Fig. 9(b).

The self-inductance of the two coils are both 149μH and the mutual inductance is 34.24 μH tested by a GWINSTEK RLC-8101G instrument with a 200 mm gap and no horizontal misalignment. Based on the following premise: the input voltage is 400 V; the transmitting coil current I_1 is 40 A; Q_2 is
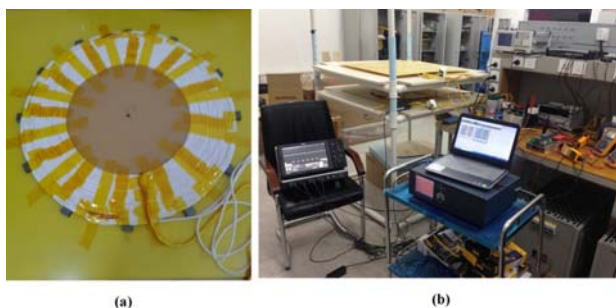
Fig. 9. The experimental prototype (a)The optimized CPs, (b)The complete experimental prototype.

TABLE I
THE EXPERIMENTAL PARAMETERS

Parameter	Value
f	20 kHz
L_p	72 μH
C_1	0.9 μF
C_{1s}	0.8 μF
L_1	149 μH
L_2	149 μH
C_2	0.43 μF

below 6; and the resonant frequency is 20 kHz [2]-[3], [13], the other parameters of the SP/S IPT system can be deduced from formulas in section III. All of the parameters are listed in Table I.

B. Experimental results

The frequency response of the prototype, measured by a VENABLE Model 3120, is shown in Fig. 10 under a 200 mm gap with no horizontal misalignment and a 160 mm horizontal misalignment. From Fig. 10, it can be easily derived that when the relative position of two pads is confirmed the voltage gain G_v is independent of R under the intrinsic resonant frequency (20 kHz). In addition, G_v decreases proportionally with the reduction of the mutual inductance. As is shown in Fig. 10, G_v with no horizontal misalignment is higher than it is at 160 mm horizontal misalignment, which clearly conforms the analysis in section III part B.

Experimental waveforms of the inverter output current and voltage are shown in Fig. 11 with a 200 mm gap and no horizontal misalignment. The inverter operates in the lagging power-factor mode. Thus, it can realize ZVS. Furthermore, the lagging phase angle is so tiny that the voltage and current can still be seen in phase, which is called the zero-phase-angle (ZPA). Hence, the inverter only needs to supply purely active power.

With a 200 mm gap and no horizontal misalignment, the measured variations of the transmitting coil current I_1 and output voltage U_R against the output power are illustrated in
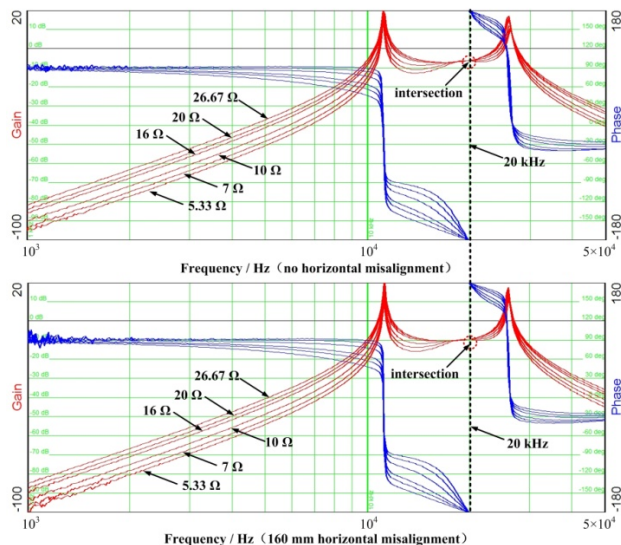

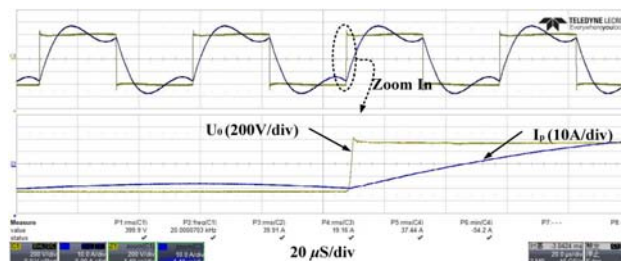Fig. 10. The frequency response of the prototype.

Fig. 11. Experimental waveforms of inverter output current and voltage.
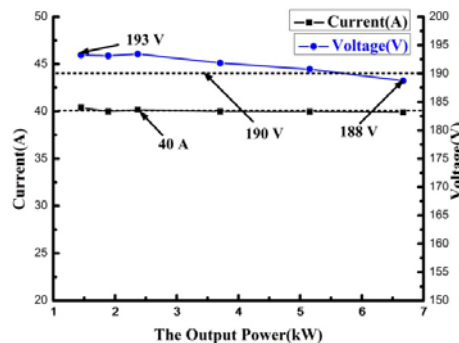

Fig. 12. The transmitting coil current and output voltage under different output power.

Fig. 12. It can be seen that the output voltage is kept approximately constant. The maximum 193 V and the minimum 188 V proves that fluctuations of the output voltage are less than 3%. The transmitting coil current stays almost the same 40 A.

With a 200 mm gap, I_1 and the output voltage under different horizontal misalignments are shown in Fig. 13. There is no doubt that I_1 is nearly constant thanks to the characteristics of the SP resonant network. The output voltage U_R is reduced as the horizontal misalignment
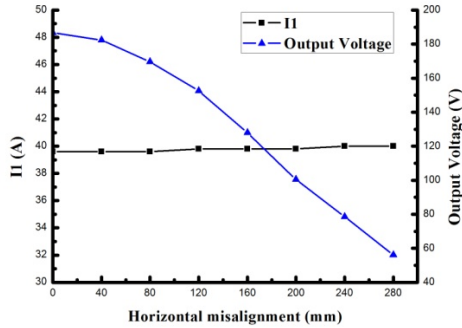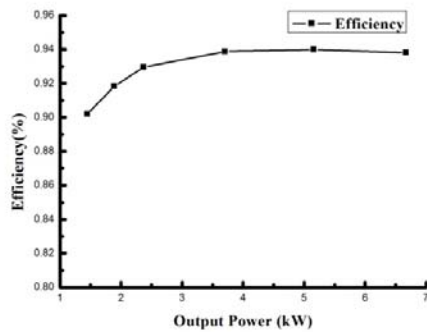
Fig. 13. I_1 and output voltage under different horizontal misalignments.

(a)

(b)

Fig. 14. (a) The experimental efficiency variation against different output power (Gap=200 mm, no horizontal misalignment); (b) maximum output power 6.6 kW with an overall DC-DC efficiency 93.8%.
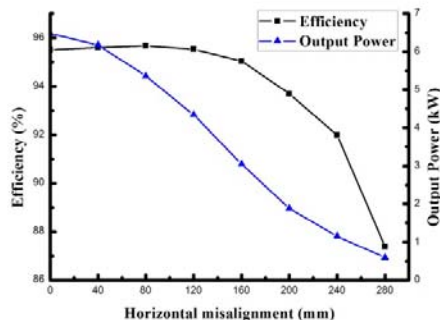

Fig. 15. Efficiency and output power as a function of horizontal misalignment.

increases, which is caused by the reduction of the mutual inductance.

The experimental efficiency (DC-DC) variation against different output powers with a 200mm gap and no horizontal misalignment was measured by a FLUKE-N5K Power Analyzer and is shown in Fig. 14(a). The whole IPT system can supply a maximum output power of about 6.6 kW with an overall DC-DC efficiency of 93.8% as shown in Fig. 14(b).

The efficiency and output power as a function of the horizontal misalignment is shown in Fig. 15. The output power is reduced with the growth of the horizontal misalignment, since the output voltage decreases at the same time. Efficiency has a small slope of decline in the beginning. When the horizontal misalignment exceeds 160 mm, it drops quickly when the output power is low enough.

V.   CONCLUSION

In this paper, further optimization of CPs is carried out based on a previous study on CPs. After the modified optimization, the magnetic coupling coefficient and power transfer capacity are both significantly improved under different horizontal or vertical misalignments. Then, a SP/S resonant compensation network for IPT systems is proposed and analyzed. Finally, a complete experimental IPT system is installed and operating at the resonant frequency (20 kHz) with the optimized 600-mm-diameter CPs. The experimental results validate the correctness and effectiveness of the optimization results and the SP/S resonant compensation network. At the position of a 200 mm gap and no horizontal misalignment, the system can supply a maximum output power of about 6.6 kW with an overall DC-DC efficiency of 93.8%.

REFERENCES

[1]   S. Li and C. C. Mi, "Wireless power transfer for electric vehicle applications," *IEEE J. Emerg. Sel. Topics Power Electron.*, Vol. 3, No. 1, pp. 4-17, Mar. 2015.

[2]   Y. Zou, X. Dai, W. Li, and Y. Sun, "Robust design optimisation for inductive power transfer systems from topology collection based on an evolutionary multi-objective algorithm," *IET Power Electronics*, Vol. 8, No. 9, pp. 1767-1776, Sep. 2015.

[3]   Y. Liao and X. Yuan, "Compensation topology for flat spiral coil inductive power transfer systems," *IET Power Electronics*, Vol. 8, No. 10, pp. 1893-1901, Oct. 2015.

[4]   B. Wang, A. P. Hu, and D. Budgett, "Maintaining middle zero voltage switching operation of parallel-parallel tuned wireless power transfer system under bifurcation," *IET Power Electronics*, Vol. 7, No. 1, pp. 78-84, Jan. 2014.

[5]   C. H. Ou, H. Liang, and W. Zhuang, "Investigating wireless charging and mobility of electric vehicles on electricity market," *IEEE Trans. Ind. Electron.*, Vol. 62, No. 5, pp. 3123-3133, May 2015.

[6]   F. Musavi and W. Eberle, "Overview of wireless power transfer technologies for electric vehicle battery charging," *IET Power Electronics*, Vol. 7, No. 1, pp. 60-66, Jan.

2014.

[7] A. Namadmalan, "Bidirectional current-fed resonant inverter for contactless energy transfer systems," *IEEE Trans. Ind. Electron.*, Vol. 62, No. 1, pp. 238-245, Jan. 2015.

[8] X. Dai and Y. Sun, "An accurate frequency tracking method based on short current detection for inductive power transfer system," *IEEE Trans. Ind. Electron.*, Vol. 61, No. 2, pp. 776-783, Feb. 2014.

[9] X. D. T. García, J. Vázquez, and P. Roncero-Sánchez, "Design, implementation issues and performance of an inductive power transfer system for electric vehicle chargers with series–series compensation," *IET Power Electronics*, Vol. 8, No. 10, pp. 1920-1930, Oct. 2015.

[10] S. C. Moon, B. C. Kim, S. Y. Cho, C. H. Ahn, and G. W. Moon, "Analysis and design of a wireless power transfer system with an intermediate coil for high efficiency," *IEEE Trans. Ind. Electron.*, Vol. 61, No. 11, pp. 5861-5870, Nov. 2014.

[11] M. Budhia, G. A. Covic, J. T. Boys, "Design and optimization of circular magnetic structures for lumped inductive power transfer systems," *IEEE Trans. Power Electron.*, Vol. 26, No. 11, pp. 3096-3108, Nov. 2011.

[12] M. Budhia, J. T. Boys, G. A. Covic, and C. Y. Huang, "Development of a single-sided flux magnetic coupler for electric vehicle IPT charging systems," *IEEE Trans. Ind. Electron.*, Vol. 60, No. 1, pp. 318-328, Jan. 2013.

[13] J. T. Boys, G. A. Covic, and A. W. Green, "Stability and control of inductively coupled power transfer systems," *IEE Proceedings - Electric Power Applications*, Vol. 147, No. 1, pp. 37-43, Jan. 2000.

[14] X. Liu; G. Wang, and W. Ding, "Efficient circuit modelling of wireless power transfer to multiple devices," *IET Power Electronics*, Vol. 7, No. 12, pp. 3017-3022, Dec. 2014.

[15] X. Yuan, Y. Zhang, Y. Wang, and Z. Li, "Output voltage control of inductive power transfer system based on extremum seeking control," *IET Power Electronics*, Vol. 8, No. 11, pp. 2290-2298, Nov. 2015.

[16] V. Prasanth and P. Bauer, "Distributed IPT systems for dynamic powering: misalignment analysis," *IEEE Trans. Ind. Electron.*, Vol. 61, No. 11, pp. 6013-6021, Nov. 2014.

[17] M. L. G. Kissin, C. Y. Huang, G. A. Covic, and J. T. Boys, "Detection of the tuned point of a fixed-frequency LCL resonant power supply," *IEEE Trans. Power Electron.*, Vol. 24, No. 4, pp. 1140-1143, Apr. 2009.

[18] D. A. G. Pedder, A. D. Brown, and J. A. Skinner, "A contactless electrical energy transmission system," *IEEE Trans. Ind. Electron.*, Vol. 46, No. 1, pp. 23-30, Feb. 1999.

[19] X. Liu and S. Y. Hui, "Optimal design of a hybrid winding structure for planar contactless battery charging platform," *IEEE Trans. Power Electron.*, Vol. 23, No. 1, pp. 455-463, Jan. 2008.

[20] M. Dockhorn, D. Kurschner, and R. Mecke, "Contactless power transmission with new secondary converter topology," in *13th Power Electronics and Motion Control Conference (EPE-PEMC)*, pp. 1734-1739, Sep. 2008.

[21] S. Valtchev, B. Borges, K. Brandisky, and J. B. Klaassens, "Resonant contactless energy transfer with improved efficiency," *IEEE Trans. Power Electron.*, Vol. 24, No. 3, pp. 685-699, Mar. 2009.

[22] C.-G. Kim, D.-H. Seo, J.-S. You, J.-H. Park, and B. H. Cho, "Design of a contactless battery charger for cellular phone," *IEEE Trans. Ind. Electron.*, Vol. 48, No. 6, pp. 1238-1247, Dec. 2001.

[23] N. Liu and T. G. Habetler, "Design of a universal inductive charger for multiple electric vehicle models," *IEEE Trans. Power Electron.*, Vol. 30, No. 11, pp. 6378-6390, Nov. 2015.

[24] A. Zaheer, H. Hao, G. A. Covic, and D. Kacprzak, "Investigation of multiple decoupled coil primary pad topologies in lumped IPT systems for interoperable electric vehicle charging," *IEEE Trans. Power Electron.*, Vol. 30, No. 4, pp. 1937-1955, Apr. 2015.

[25] X. Li and A. K. S. Bhat, "A utility-interfaced phase-modulated high-frequency isolated dual LCL DC/AC converter," *IEEE Trans. Ind. Electron.*, Vol. 59, No. 2, pp. 1008-1019, Feb. 2012.

[26] A. Abdolkhani and A. P. Hu, "Improved autonomous current-fed push-pull resonant inverter," *IET Power Electronics*, Vol. 7, No. 8, pp. 2103-2110, Aug. 2014.

[27] R. M. Linus and P. Damodharan, "Maximum power point tracking method using a modified perturb and observe algorithm for grid connected wind energy conversion systems," *IET Renewable Power Generation*, Vol. 9, No. 6, pp. 682-689, Aug. 2015.

[28] H. Hao, G. A. Covic, and J. T. Boys, "A parallel topology for inductive power transfer power supplies," *IEEE Trans. Power Electron.*, Vol. 29, No. 3, pp. 1140-1151, Mar. 2014.

[29] W. Zhang, S. C. Wong, C. K. Tse, and Q. Chen, "Analysis and comparison of secondary series- and parallel-compensated inductive power transfer systems operating for optimal efficiency and load-independent voltage-transfer ratio," *IEEE Trans. Power Electron.*, Vol. 29, No. 6, pp. 2979-2990, Jun. 2014.

[30] P. Vecchia, "Guidelines for limiting exposure to time-varying electric, magnetic, and electromagnetic fields (up to 300 GHz)," *International Commission on Non-Ionizing Radiation Protection (ICNIRP)*, Vol. 74, No. 4, pp. 494-522, Apr. 1998.

[31] *Maximum exposure levels to radiofrequency fields: 3 kHz to 300 GHz*, Australian Radiation Protection and Nuclear Safety Agency (ARPANSA), 2002.
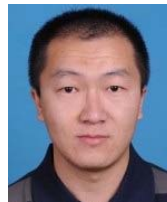
Chenglian Ma received his M.S. degree in Electrical Engineering from Northeast Dianli University, Jilin, China, in 2009. He is presently working towards his Ph.D. degree in the School of Electrical and Electronic Engineering, North China Electric Power University, Beijing, China. His current research interests include wireless power transfer, power system safety operation and control, and HVDC connected issues.

Shukun Ge received his B.S. degree from the Heilongjiang University of Science and Technology, Heilongjiang, China, in 2014. He is presently working towards his M.S. degree in the Department of Electrical Engineering, Northeast Dianli University, Jilin, China. His current research interest include wireless power transfer (WPT).

Ying Guo received his B.S. degree from the Qingdao Technological University, Qingdao, China, in 2012; and his M.S. degree from the Department of Electrical Engineering, Northeast Dianli University, Jilin, China, in 2016. He is presently working for the State Grid Zibo Power Supply Company, Zibo, China. His current research interest includes wireless power transfer (WPT).

Li Sun received her M.S. degree in Electrical Engineering from Northeast Dianli University, Jilin, China, in 2008. She is presently working towards her Ph.D. degree in Electrical and Electronic Engineering, North China Electric Power University, Beijing, China. Her current research interests include high voltage direct current transmission technology.

Chuang Liu received his M.S. degree in Electrical Engineering from Northeast Dianli University, Jilin, China, in 2009; and his Ph.D. degree from the Harbin Institute of Technology, Harbin, China, in 2013. From 2010 to 2012, he was with Future Energy Electronics Center (FEEC), Virginia Tech, Blacksburg, VA, USA, as a Visiting Ph.D. Student, with support from the Chinese Scholarship Council. Since 2013, he has been an Associate Professor in the School of Electrical Engineering, Northeast Dianli University. His current research interests include solid-state substations based on power electronics transformers for future hybrid ac/dc power grids, PHEV/PEV smart parking lot/building charging systems, battery energy storage systems, and wireless power transfer.